Introduction to EELS

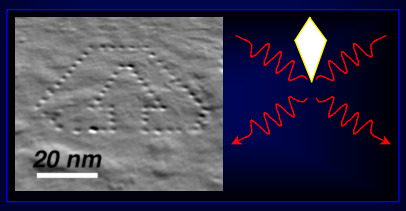

Nestor J. Zaluzec

zaluzec@microscopy.com

zaluzec@aaem.amc.anl.gov

Brief Review of Energy Loss Processes

Instrumentation: Detector Systems

Instrumentation: AEM Systems

Data Analysis and Quantification:

Advanced Topics

Brief Review of Energy Loss Processes

Electron Excitation of Inner Shell & Continuum Processes
Spectral Shapes
Notation of Edges
Electron Scattering Angular Distributions

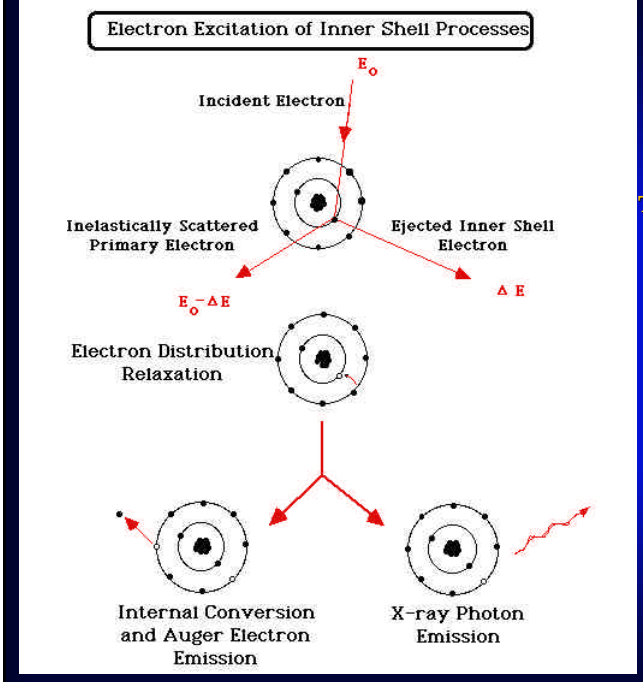

The Emission Process:

1-Excitation,
2-Relaxation,
3-Emission

Electron Energy Loss Spectroscopy

Measure the changes in the energy distribution of an electron beam transmitted through a *thin* specimen.

Each type of interaction between the electron beam and the specimen produces a *characteristic* change in the energy and angular distribution of scattered electrons.

The energy loss process is the *primary* interaction event. All other sources of analytical information (i.e. X-rays, Auger electrons, etc.) are *secondary* products of the initial inelastic event. Thus, EELS has the highest potential yield of information/inelastic event

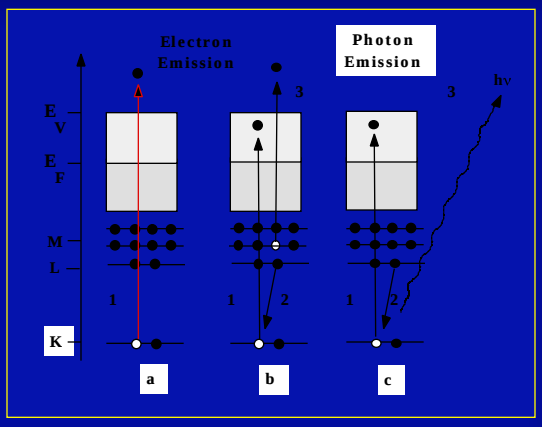

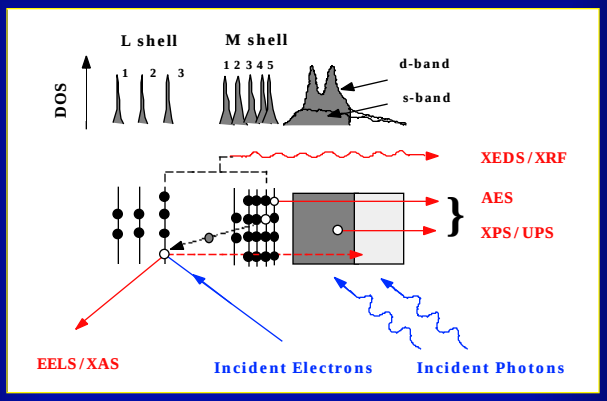

Schematic Diagram Illustrating Sources of Inelastic Scattering Signals

Experimental XEDS, XPS, and EELS data from the Copper L shell. Note the differences in energy resolution, and spectral features.

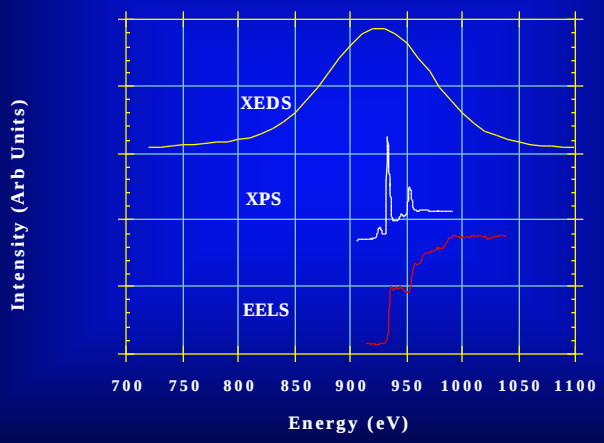

Edges for EELS Microanalysis
(0 - 3 keV)

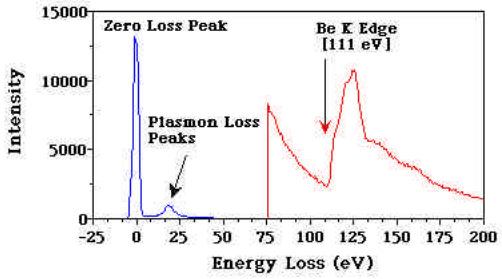

Table 1. Edges Suitable for EELS Microanalysis
for the Energy Range 0-3 keV

Atomic Number	Inner Shell	Spectroscopic Notation
Z = 1-11	K	1s
Z = 12-17	K L_3,L_2,L_1	1s $2p_{3/2},2p_{1/2}$,2s
Z = 19-45	L_3,L_2,L_1 M_{54},M_{32},M_1	$2p_{3/2}$,.--> $3d_{5/2},3d_{3/2}$, $3d_{1/2}$, $3p_{3/2},3p_{1/2}$,3s
Z = 46-79	M_{54},M_{32},M_1 N_{45},N_{32},N_1 O_{32},O_1	$3d_{5/2}$,..--> $4d_{5/2},4d_{3/2},4d_{1/2}$, $4p_{3/2},4p_{1/2}$,4s $5p_{3/2},5p_{1/2}$,5s
Z > 80	N_{67},N_{45},N_{32},N_1 O_{45},O_{32},O_1	$4f_{7/2}$,.--> $5p_{3/2}$.-->

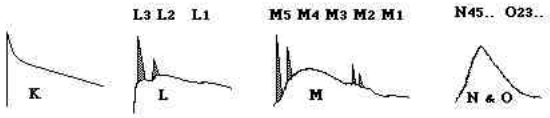

Figure 5. Schematic illustration of K, L, M, N and O Edge shapes, the "white lines" sometimes detected on L and M shells are shown shaded peaks at the edge onsets. In all sketches the background shape has been omitted for clarity. These profiles should be compared with experimental profiles of figure 6.

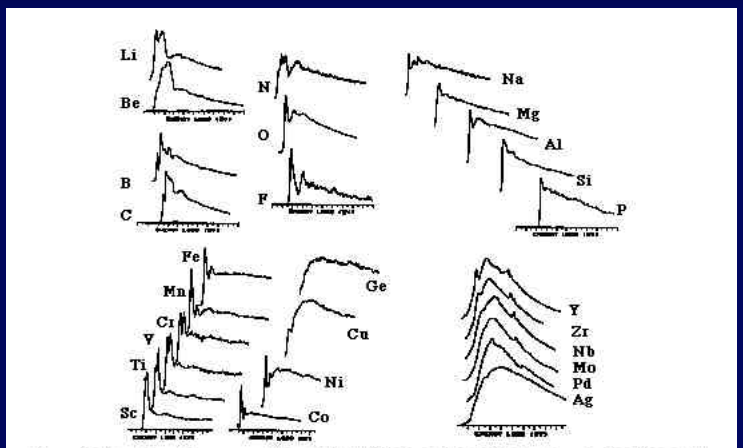

Figure 6. Selection of representative K-Shell [Li, Be, B, C, N, O, F, Na, Mg, Al, Si, P]; L-shell [Sc, Ti, V, Cr, Mn, Fe, Co, Ni, Cu, Ge] and M-shell [Y, Zr, Nb, Mo, Pd, Ag] experimental spectral profiles (all background subtracted).

Comparision Light Element Spectroscopy Resolution XEDS vs EELS

Comparision of WL XEDS Detector and EELS spectra taken from the same NiO specimen

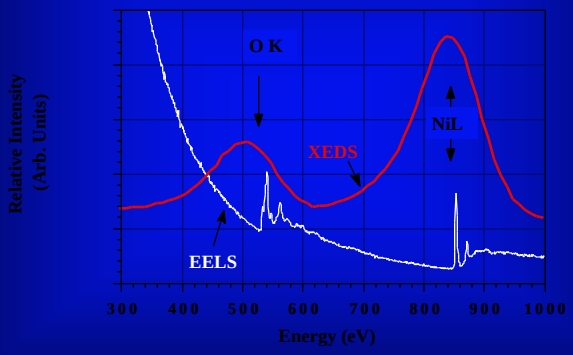

Note the enhanced spectral information in the EELS data. Vertical scale is arbitrary and chozen for clarity of presentation.

Type of Electron Scattering	Angular Range	Energy Loss
Unscattered	0	0
Elastic	10's-100's mR	~0
Phonon	10's-100's mR	<.025 eV
Inelastic	10's mR	everything else

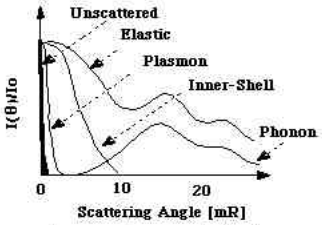

Amorphous Solids

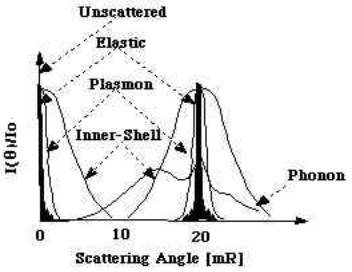

Crystalline Solids

Elastic Scattering

Single Atoms:

$$I(\theta) \sim |f(\theta)|^2 = |f_o|^2 \bullet \frac{1}{(\theta^2 + \theta_o^2)^2}$$

$$\theta_o = \frac{1}{2\pi(0.885 a_o Z^{-1/3})}$$

Amorphous Solids:

$$I(\theta) \sim |f(\theta)|^2 \bullet \left(1 + \frac{\sin(kR)}{kR}\right)$$

$$k = \frac{4\pi}{\lambda} \sin(\theta)$$

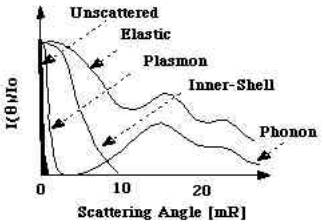

Elastic Scattering

Crystalline Solids:

$$I(\theta) \sim |F(hkl)|^2$$

$$F(hkl) = \sum_j f_j(\theta)\ e^{(-2\pi i \vec{k}\cdot\vec{r})}$$

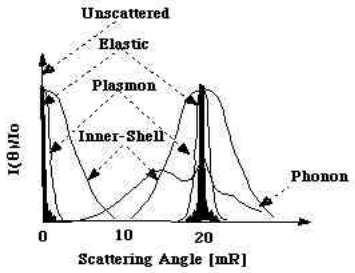

Phonons:

$$I(\theta) \sim |f(\theta)|^2 \cdot \{1 - e^{-2M}\}$$

$$M = \frac{8\pi \langle u^2 \rangle \sin(\theta)}{\lambda}$$

Inelastic:

$$I(\theta) = \Gamma(\delta E, \theta) \cdot \frac{1}{\theta^2 + \theta_E^2}$$

$$\theta_E = \frac{\Delta E}{2\gamma_o T_o} \qquad \gamma_o = \frac{1}{\sqrt{1-\beta^2}}$$

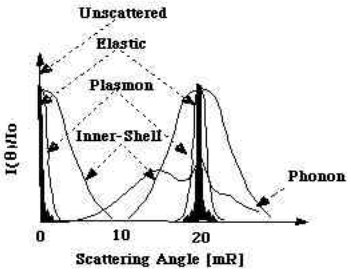

$\Gamma(\delta E,\theta)$: Imaginary Part of the Complex Dielectric constant(ε)
: Generalized Oscillator Strength

Instrumentation: Detector Systems

Energy Loss Spectrometers
- Basic Principles
- Electrostatic/Electromagnetic
- Serial/Parallel Detector Systems
- Spectral Artifacts

Multichannel Analyzers

Force (F) and displacements (X) on electrons by different types of fields yields a deflection in their trajectory. In a uniform field region the electrons drift at a characteristic radius (R).

Electrostatic

$$\vec{F_E} = q\,\vec{E} \qquad X_E = \frac{1}{2}\frac{qEL^2}{m_o v^2} \qquad R_E = \frac{m_o v^2}{qE}$$

Electromagnetic

$$\vec{F_B} = q\left[\vec{v} \times \vec{B}\right] \qquad X_B = \frac{1}{2}\frac{qBL^2}{m_o v} \qquad R_B = \frac{m_o v}{qB}$$

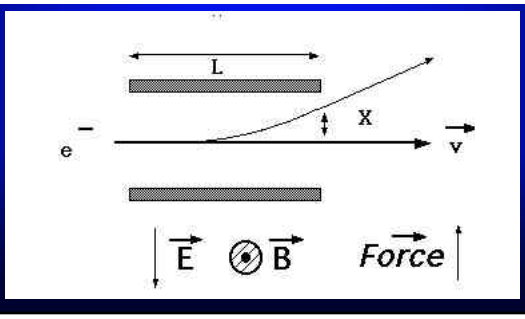

Basic Spectrometer

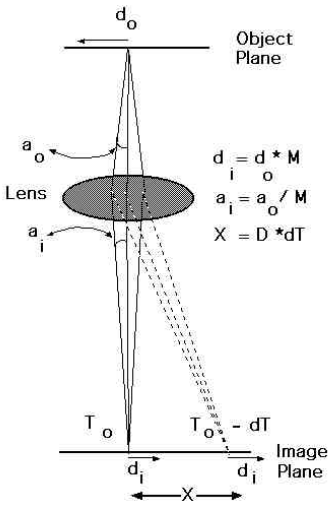

Types of Electron Spectrometers:

Electrostatic:	**Mollenstedt**
Electrostatic/magnetic:	**Wien, Castaing-Henry**
Electromagnetic:	**Cylindrical, Omega, Sector**

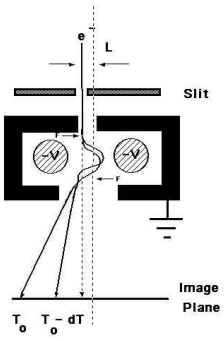

Mollenstedt Analyzer

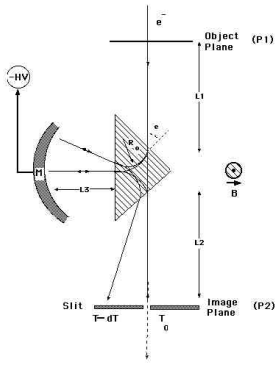

Castaing-Henry Filte

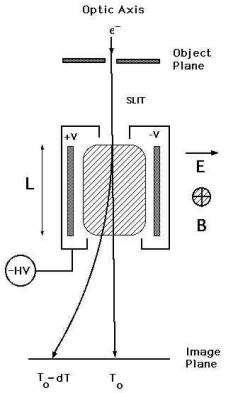

Wien Filter

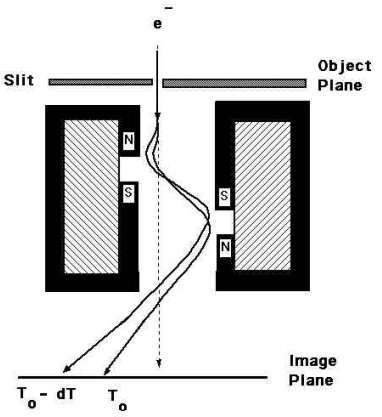

Cylindrical Magnetic Analyzer

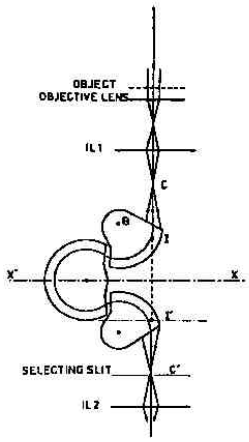

Omega Filter

Magnet Sector Analyzer

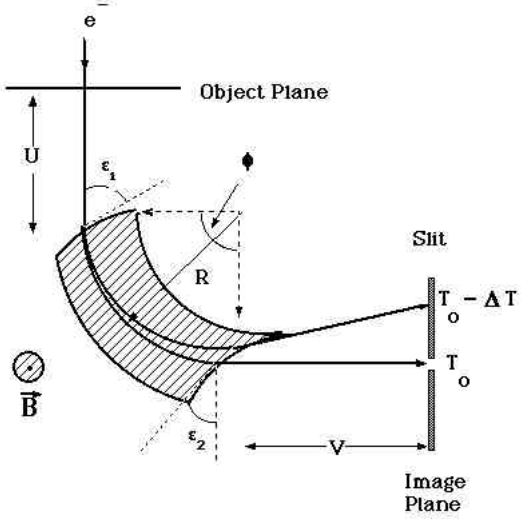

Data Collection Serial Detectors

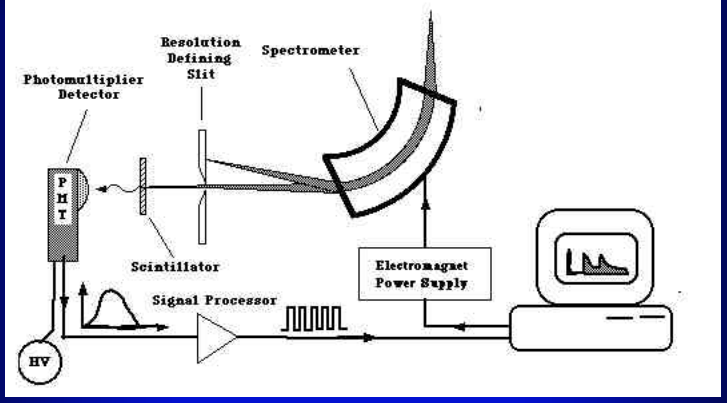

Major Components

Spectrometer
Computer or Multi-Channel Scaler
Magnet Power Supply
Slit/Scintillator/PMT Detector
Signal Processor

Data Collection Parallel Detectors

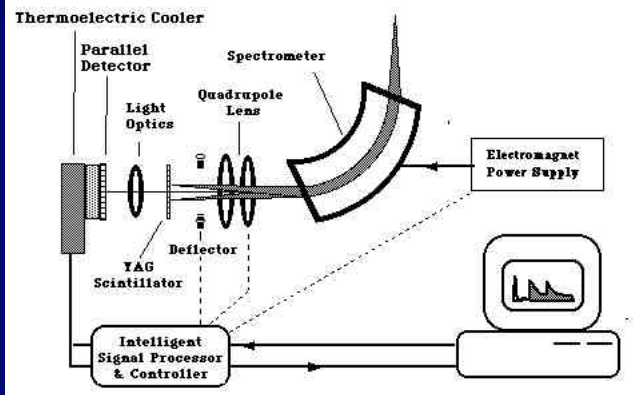

Major Components

Spectrometer
Computer
Magnet Power Supply
Quadrupole Lenses, Deflectors, & Power Supplies
Scintillator, Parallel Detector, Thermoelectric Cooler
Intelligent Signal Processor

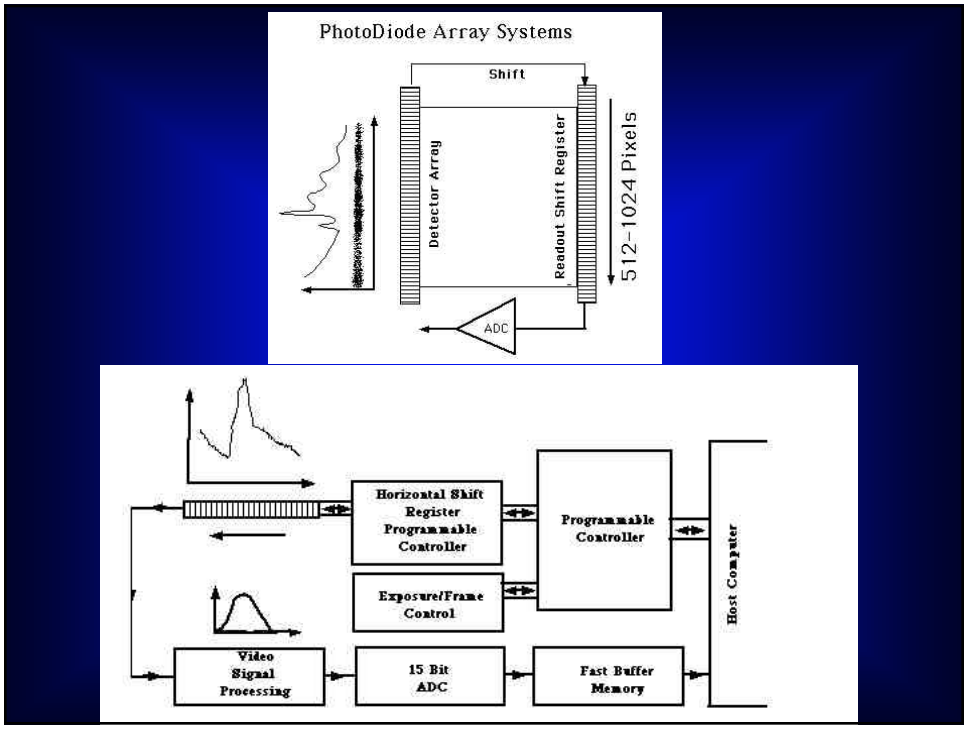
PhotoDiode Array Systems
Shift
Detector Array
Readout Shift Register
512-1024 Pixels
ADC
Horizontal Shift Register Programmable Controller
Programmable Controller
Exposure/Frame Control
Host Computer
Video Signal Processing
15 Bit ADC
Fast Buffer Memory

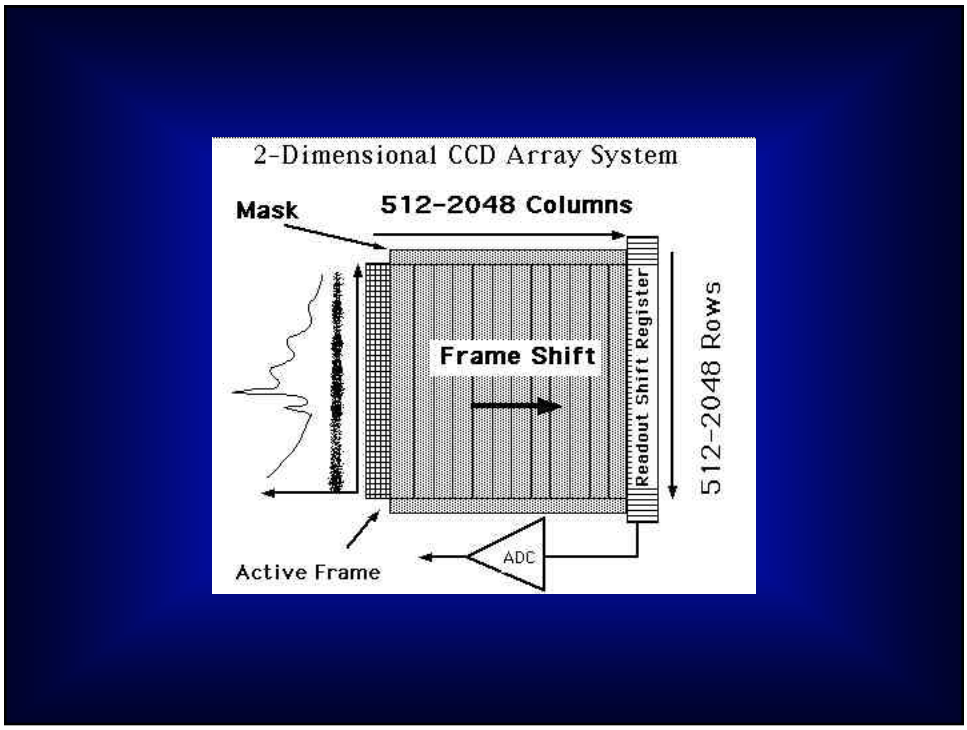
2-Dimensional CCD Array System
Mask
512-2048 Columns
Frame Shift
Readout Shift Register
512-2048 Rows
ADC
Active Frame

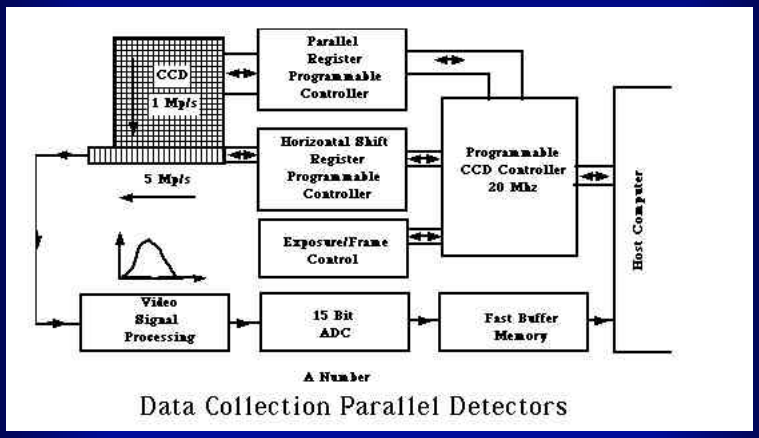

Data Collection Parallel Detectors

Serial vs Parallel

Serial Advantages	Parallel Advantages
•Simple operation & control •Large Dynamic Range •Effective gain changes can be programmed into a spectral scan by controling PMT HV by computer which extends dynamic range •Excellent Signal/Noise •Directly adaptable to STEM/TEM serial energy filtered imaging	•Rapid & efficient data collection •Lower dose irradiation of the specimen is possible •Large energy interval collection within a single readout •Energy filtered imaging possible with 2D arrays in TEM
Serial Disadvantages	**Parallel Disadvantages**
•Single energy interval per readout •Long data collection times •Large dose irradiations of the specimen •PMT detectors may exhibit saturation and after-glow from zero loss peak •Electromagnetic scanning will affect energy calibration •Stray AC field effects can be important •Improper slit design can result in "hole count" background •Scintillator performance will decay with damage/contamination	•Complicated control requires sophisticated programming •Limited pixel well capacity limits the dynamic range within a readout •Detector after image on high intensity irradiations requires multiple readouts to clear. •ReadOut Noise:Fixed pattern and Leakage exists in all readouts •Imaging requires additional lenses or computer processing to select an energy window. •Channel to Channel gain variation must be normalized out

Comparison of Data Collection Times
1000 Channel Spectrum @ DQE=1

Parallel	Serial*
1 sec	16.7 minutes
1 minute	16.7 hours
1 hour	41.6 days
1 day	2.74 years

* Unfair comparison but it gives you an order of magnitude estimate of the times involved

Data Analysis and Quantification:

Spectral Processing
Thin Film Quantification Methods
Specimen Thickness Effects

Measurement of Parameters required for EELS Quantification

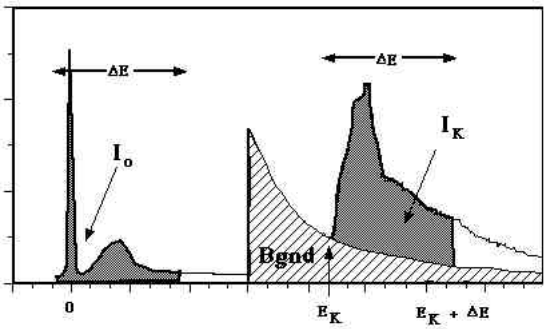

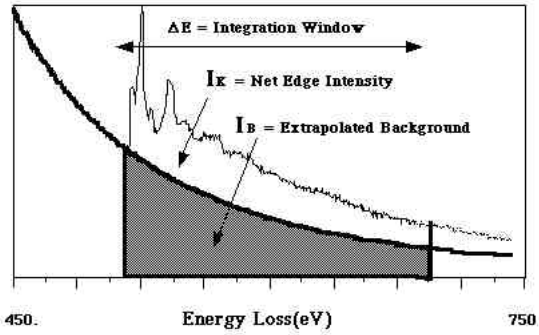

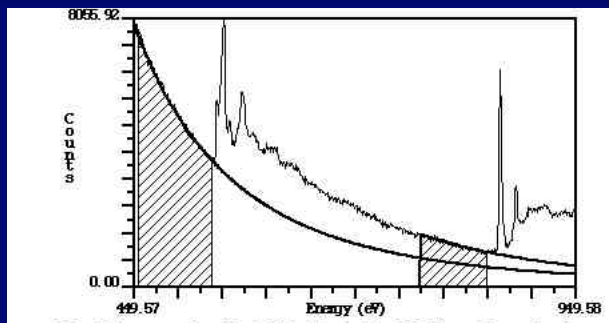

Most Frequently Used Model in the Medium Loss Regime

$$I_{Bgnd} = A\ E^{-R}$$

$2 \leq R \leq 7$ typical values for 200 eV < E < 1500 eV

Other Background Models Used are Phenomenological

N^{th} Order Polynominal & Log-Polynominal mainly used < 200 eV Loss

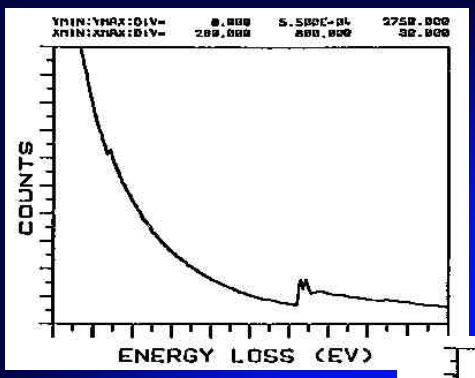

$M_{23}C_6$ in Steel : Spectral Overlap

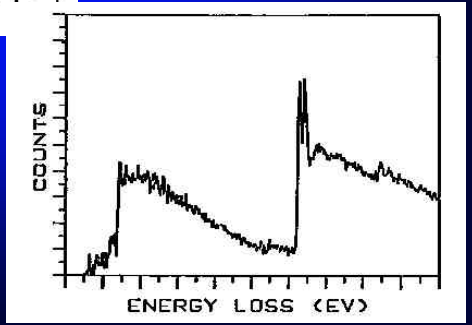

Spectral OverLap Problems also exist in EELS

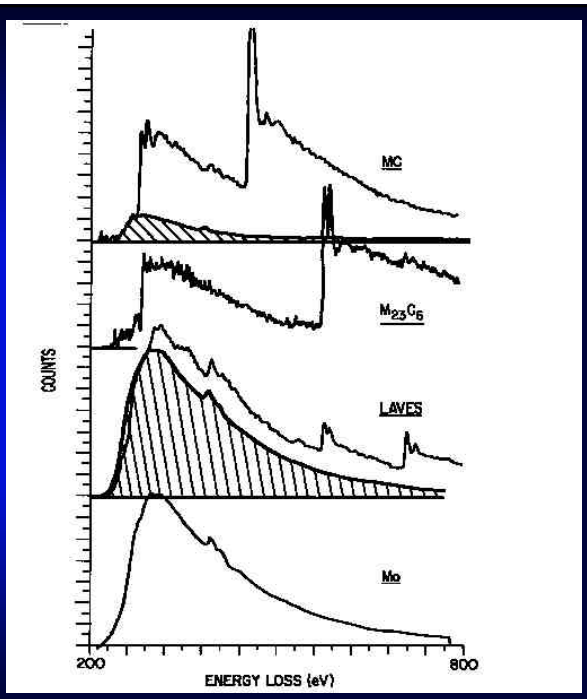

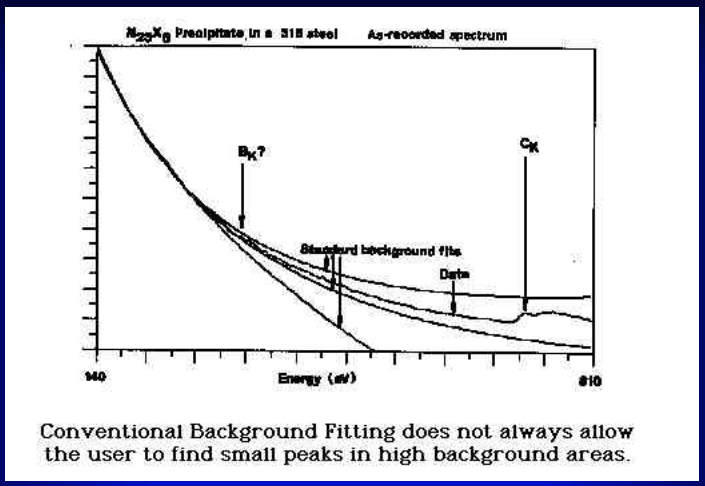

Conventional Background Fitting does not always allow the user to find small peaks in high background areas.

Two Related Methods are sometimes used:

Second Difference Filtering (Shuman etal MAS,1983**)**

Record 3 Energy Loss Spectra which are displaced in energy by dE Mathematically combine in computer to form the Second Difference (SD) Spectrum

$$SD(E) = I_1(E-dE) - 2\,I_2(E) + I_3(E+dE)$$

Spectrum has the appearance of a derivitive, removes channel to channel gain variation in parallel EELS and slowly varying backgrounds. Sharp features are enhanced in visibility.

Digital Filtering

This is related to a simple numerical differentiation of a single spectrum

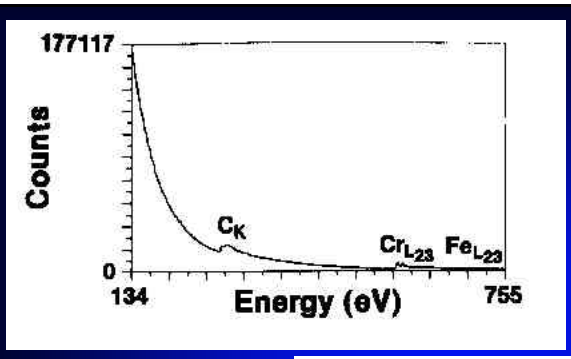

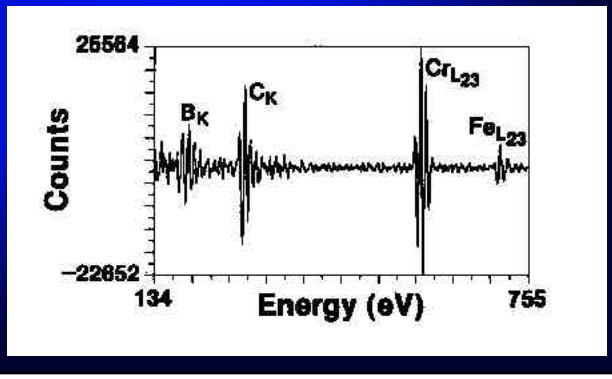

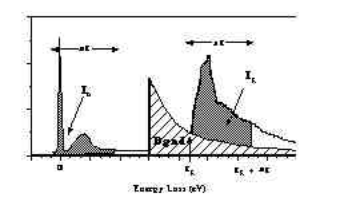

$I_k = P_k * I_o$

I_k = Number of electron having excited a kth inner shell

P_k = Probability of excitation of the kth shell

I_o = Incident electron current

$P_k = N \sigma_k$

N = Number of atoms of the element analyzed

σ_k = Ionization cross-section for the kth shell

$$N = \frac{I_k}{\sigma_k I_o}$$

Alternatively;

Consider the ratio of Intensities of any two Edges in the same spectrum I_A and I_B

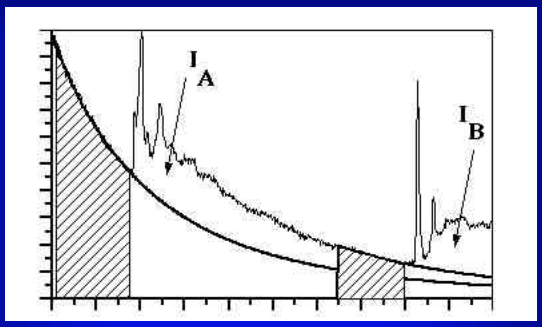

Invoke the Ratio Method and obtain the exact equation:

$$\frac{I_A}{I_B} = \frac{\sigma_A}{\sigma_B} \frac{N_A}{N_B}$$

Note the similiarity of this equation with that of Thin Film XEDS

But in the real world the assumptions used in the above simple arguments are never realized:

- Measure all scattered electrons ($\beta=\pi=180^0$)
- Integration over all energy Losses

Because we must measure over a finite energy window (δE) we modify the expression to:

$$N_A = \frac{I_A(\delta E)}{\sigma_A(\delta E) * I_0}$$

we also measure over a finite angular window (β) and therefore, we modify the expression to:

$$N_A = \frac{I_A(\delta E, \beta)}{\sigma_A(\delta E, \beta) * I_0}$$

and the ratio equation becomes:

$$\frac{N_A}{N_B} = k_{AB} \frac{I_A(\delta E, \beta)}{I_B(\delta E, \beta)}$$

with

$$k_{AB} = \frac{\sigma_B(\delta E, \beta)}{\sigma_A(\delta E, \beta)}$$

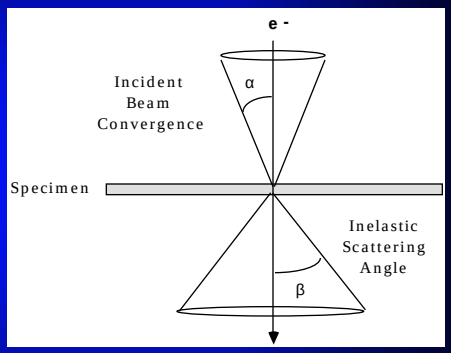

By measuring $\mathcal{N}$ edges we have $\mathcal{N}-1$ equations, if we invoke the argument that the compositions must sum to unity

$$\sum_{i=1}^{\mathcal{N}} C_i = 1$$

we arrive at a set of $\mathcal{N}$ equations and $\mathcal{N}$ unknowns which can be solved by simple algebra.

For example:

- if $N_A/N_B = 2.$; then $N_A = 2\,N_B$
- if $N_A + N_B = 1$; then $3N_B = 1$ or $N_B = 0.33$
- and $N_A = 1 - N_B = 0.67$

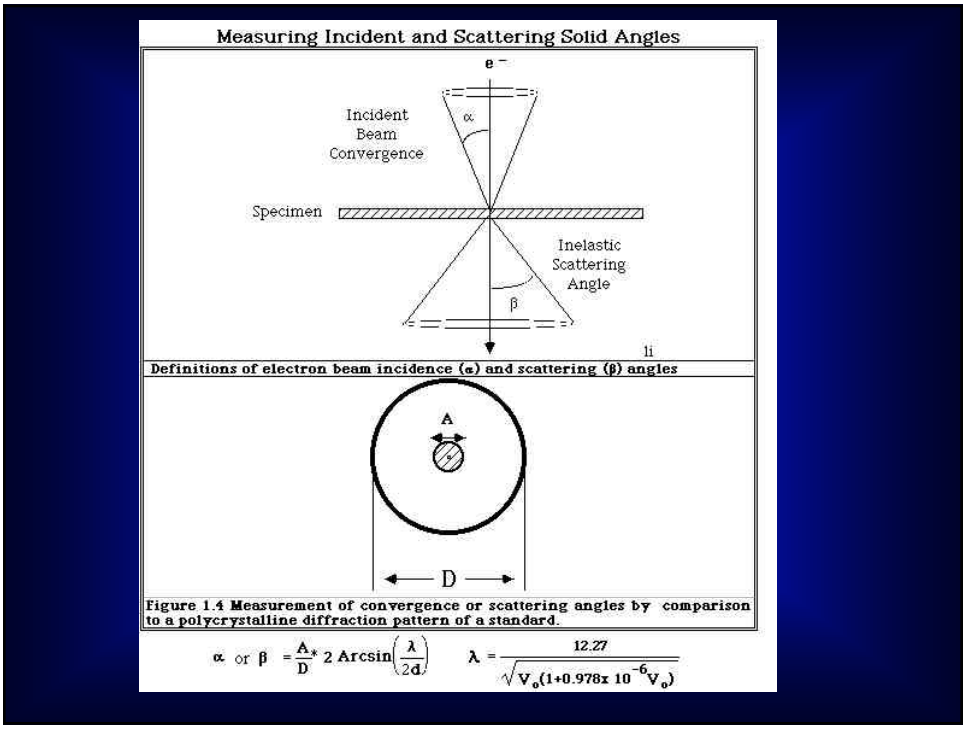

Problems in EELS Quantification
Cross-section Calculations

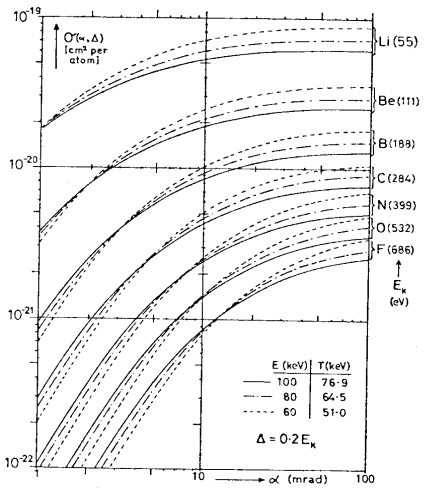

Fig. 3. K-shell partial cross-sections for first-row elements with $\Delta = 0.2\,E_K$ and incident electron energies of 60, 80 and 100 keV.

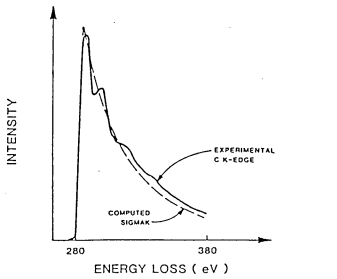

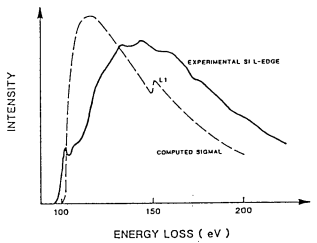

Figure 5 Comparison of an experimental L edge profile with the equivalent profile calculated by using the SIGMAL model.

Problems In EELS Quantification
Collection Angle Errors

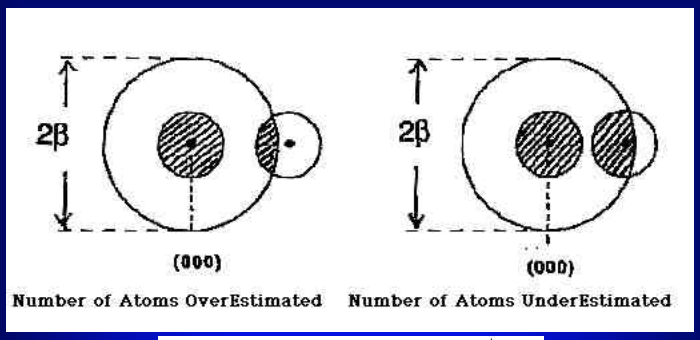

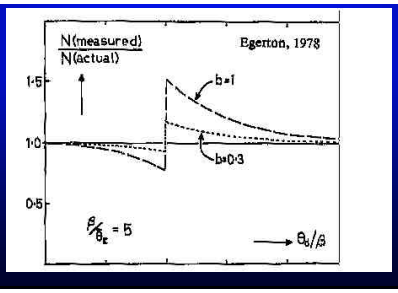

Problems In EELS Quantification
Multiple Scattering

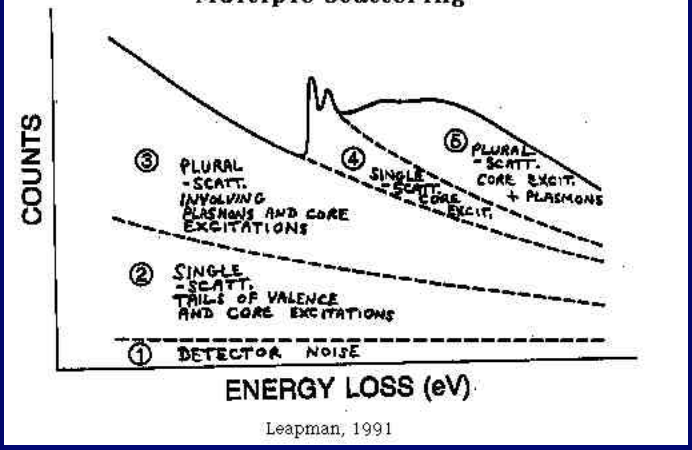

Leapman, 1991

Effects of Specimen Thickness

- **Multiple Scattering**
  - **Low Loss**
  - **Core Loss -Visiblity**
  - **Quantification Effects**

Effects of Specimen Thickness

Low Loss Spectra

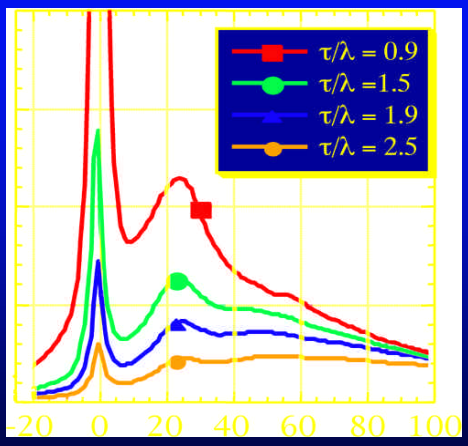

$$\frac{I_P}{I_o} = \frac{t}{\lambda} \leq 0.1$$

$$\ln\left(\frac{I_T}{I_o}\right) = \frac{t}{\lambda} \leq 1.0$$

Effects of Specimen Thickness

Core Loss Spectra

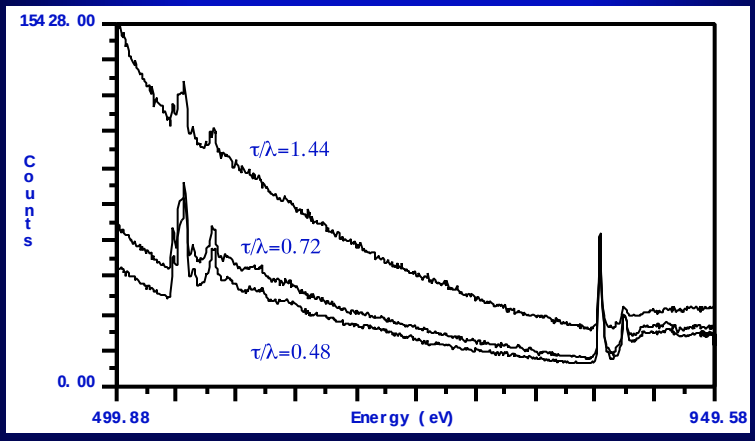

Variation in EELS Edge P/B with Thickness

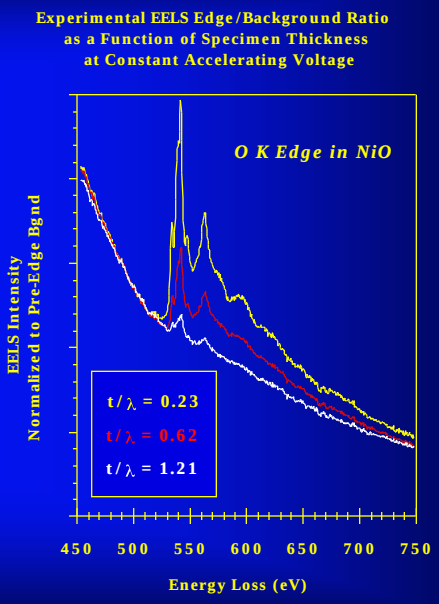

Mean Free Path

$$\lambda \approx \frac{2a_o T}{\bar{E}_m \left(1-n^{-2}\right)\cdot \ln\left[\frac{2\gamma T\theta_c}{\bar{E}_m}\right]}$$

$$T = \frac{m_o v^2}{2} = \frac{m_o c^2 \beta^2}{2} = Eo \cdot \frac{\left[1+\frac{E_o}{2m_o c^2}\right]}{\left[1+\frac{E_o}{m_o c^2}\right]^2}$$

Normalized Mean Free Path

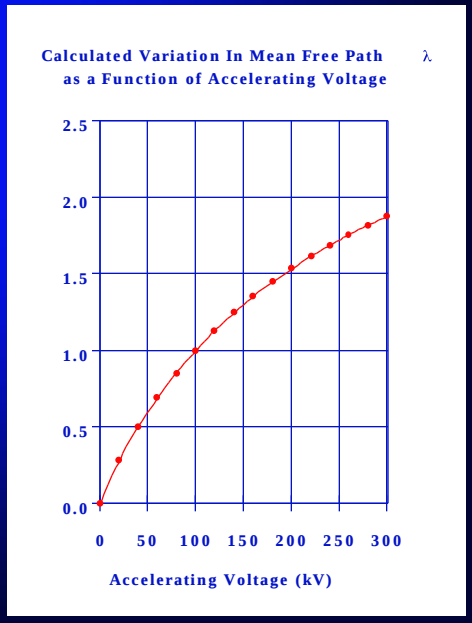

Experimental Measurement of MFP

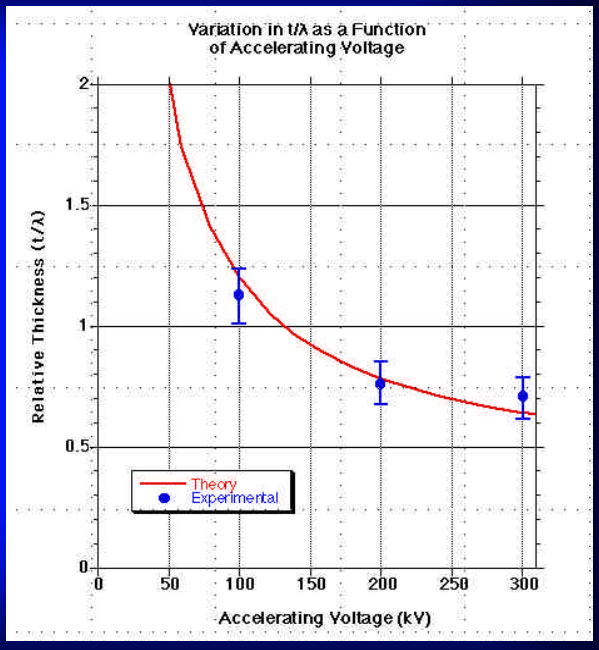

Variation in EELS Edge P/B with kV

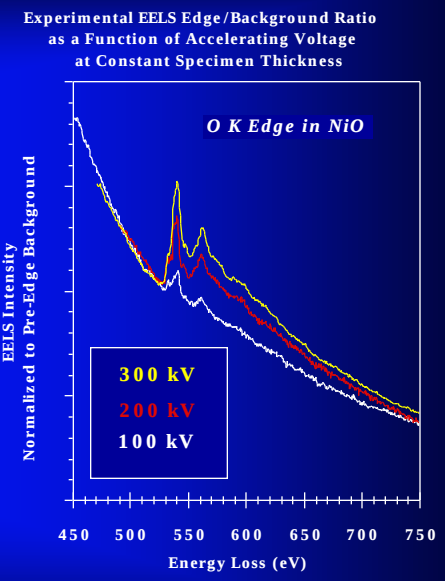

Specimen Thickness Effects on EELS

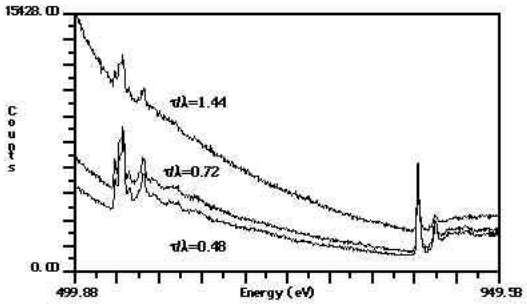

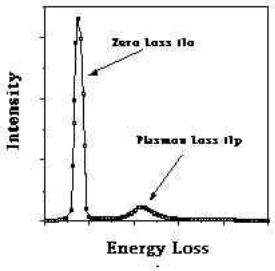

$$\frac{I_P}{I_o} = \frac{t}{\lambda} \leq 0.1$$

$$\ln\left(\frac{I_T}{I_o}\right) = \frac{t}{\lambda} \leq 1.0$$

Effects of Thickness and Voltage on EELS P/B

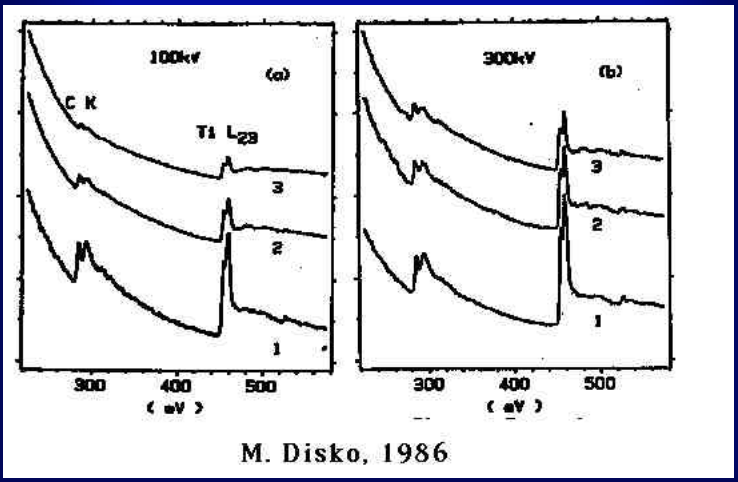

M. Disko, 1986

Deconvolution of Multiple Scattering using Leapman/Swyt Method

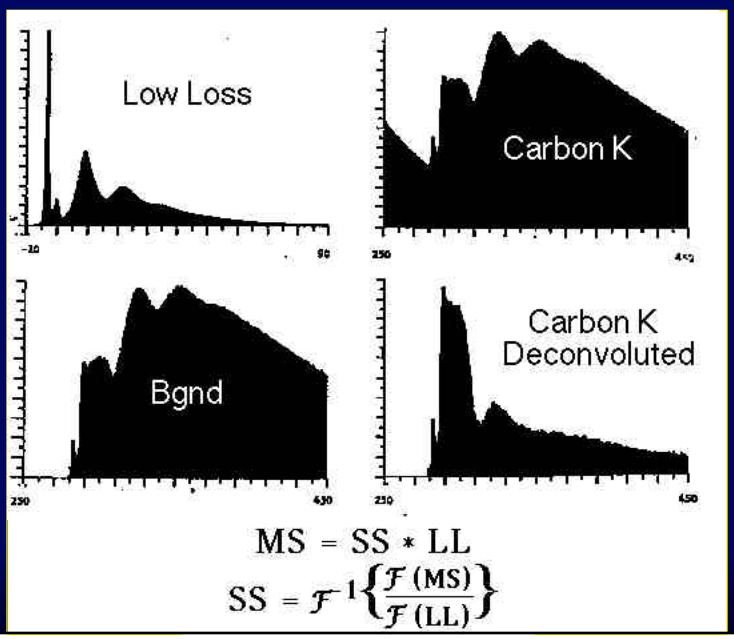

$$MS = SS * LL$$

$$SS = \mathcal{F}^{-1}\left\{\frac{\mathcal{F}(MS)}{\mathcal{F}(LL)}\right\}$$

Does Deconvolution Help Quantification?

Recall the Basic Equation

$$\frac{I_A}{I_B} = \frac{\sigma_A \; N_A}{\sigma_B \; N_B}$$

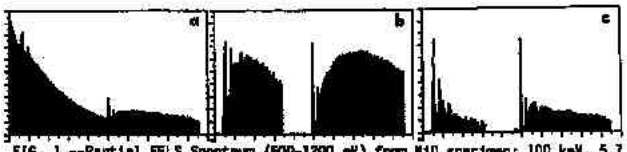

FIG. 1.--Partial EELS Spectrum (500-1200 eV) from Ni0 specimen: 100 keV, 5.7 mr scattering angle, a) unprocessed data b) background stripped, c) deconvoluted.

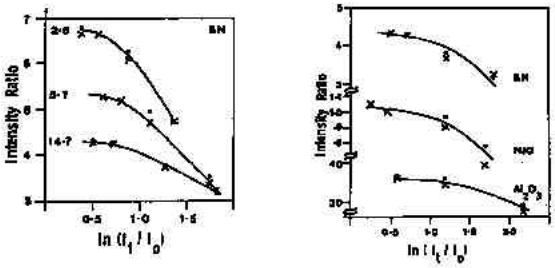

This defines a "Thin Film Approximation" for EELS i.e. $\tau/\lambda < 1.0$

Advanced Topics

- Low Loss Spectroscopy
  - Plasmon Losses Studies
  - Dielectric Properties
- Core Loss Spectroscopy
  - Near Edge Structure
  - Extended Fine Structure
- Radiation Damage

EELS Measurements of Valence Electron Densities

$$\text{Plasmon Energy} = E_p = \hbar\omega_p = \sqrt{\frac{\hbar^2 e^2}{\eta m \varepsilon_o}}$$

e is the elctron charge,
m its mass,
ε_o the vacuum dielectric constant,
$\hbar$ = Planck's constant/2π
η the valence electron density

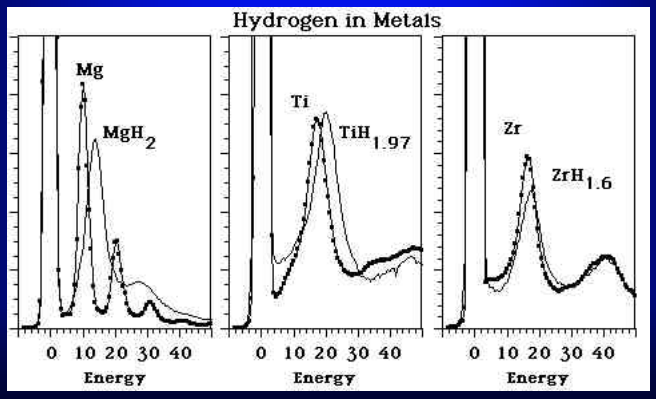

Table 2 Experimental and Calculated Plasmon Shifts in Selected Metal-Hydrogen Systems

Material	Expt. E_p (eV)	Calculated FEM	ΔE_p/H/M Expt.	ΔE_p/H/M FEM Calc.
Group II				
Mg	10.0 ± 0.5	10.90	2.1± 0.7	1.24
MgH_2	14.2± 0.5	13.38		
Group III				
Sc	14 ± 2 eV	12.87	1.6± 0.7	1.50
ScH_2	17.2 ± 0.5	15.87		
Y	12.5 ± 0.2	11.19	1.4 ± 0.7	1.41
YH_2	15.3 ± 0.5	14.0		
Group IV				
Ti	17.2 ± 0.5	17.69	1.4± 0.7	0.87
$TiH_{1.97}$	20.0 ± 0.5	19.4		
Zr	16.6± 0.5	15.37	0.9± 0.7	0.91
$ZrH_{1.6}$	18.1± 0.5	16.83		
Group V				
V	22.0 ± 0.5	22.29	0.0	0.3
$VH_{0.5}$	22.0 ± 0.5	22.44		
PseudoGroup VI				
FeTi	22.0± 0.5	25.04/21.9*	0.0	-0.84/-0.3*
FeTiH(β)	22.0± 0.5	24.65/21.8*		
$FeTiH_2$(γ)	22.0± 0.5	24.15/21.5*		

* Calculated using modified FEM with $m_s = m_e$ and $m_d = 1.9\ m_e$

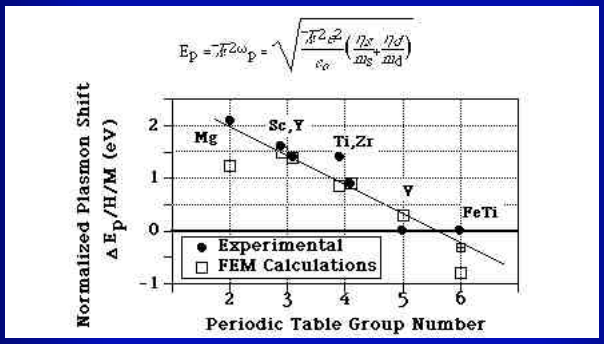

Information in Core-Loss Profiles

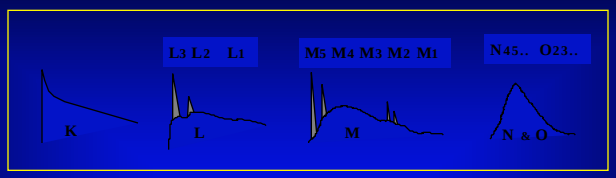

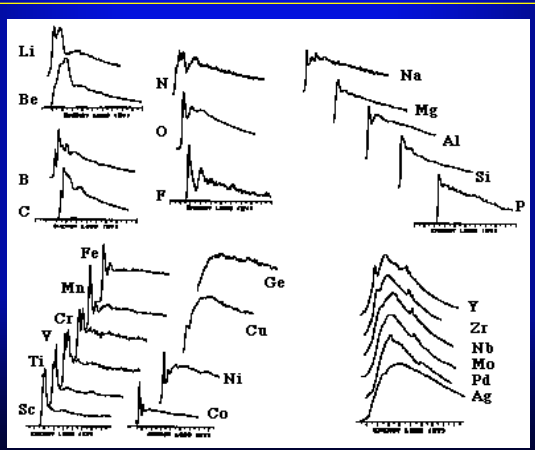

Oxygen K Shell in superconducting and non-superconducting specimens in the $Bi_2Sr_2Ca_{n-1}Cu_nO_x$ system. Note the disappearance of the pre-edge peak in the non-superconducting specimen.

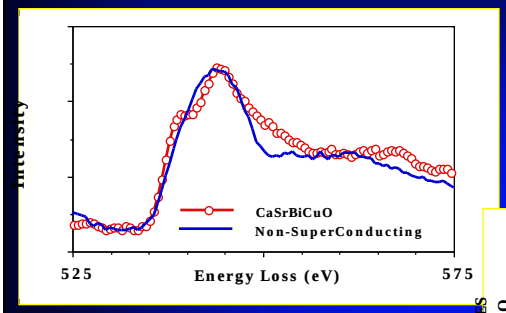

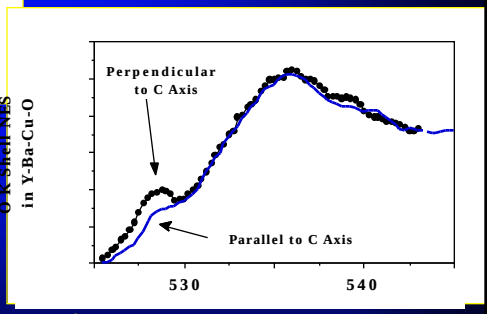

Orientation dependance of the O K shell in $Y_1Ba_2Cu_3O_{7-\delta}$. The intensity variation of the pre-edge peak indicates that the hole state just above the Fermi level has $\rho_{x,y}$ symmetry. Parallel and perpendicular here refer to the momentum transfer directions which are by conservation perpendicular to the incident beam directions

Dielectric Function Measurements

As the fast electron looses energy in transmission through the specimen its interaction (i.e. the intensity of the measured loss spectrum I(E)) can be related to energy loss probability P(E,θ) which can be described using dielectric theory as :

$$I(E) = \int P(E,\theta)\, dE\, d\Omega$$

$$I(E) = \text{constant} * \frac{t}{E_O} \int \left(\frac{1}{\theta^2 + \theta_E^2}\right) * \text{Im}\left(-\varepsilon^{-1}(E,q)\right) dE\, d\Omega$$

where $d\Omega$ is the unit solid angle, t the specimen thickness, E_o the electron kinetic energy, q the momentum vector, θ and θ_E the characteristic electron scattering angles and $\varepsilon = (\varepsilon_1 + i\,\varepsilon_2)$ is the dielectric function of the solid. By applying a Kramers-Kronig analysis (KKA) to the energy loss function ($\text{Im}(\varepsilon(E,q)^{-1})$), the real part $\text{Re}(\varepsilon^{-1})$ of ε can be computed from intensity measurements and then the real and imaginary parts (ε_1, ε_2) of the dielectric function determined. From these, one can then calculate the optical constants (refractive index η, absorption index κ, and reflectivity R) for the material.

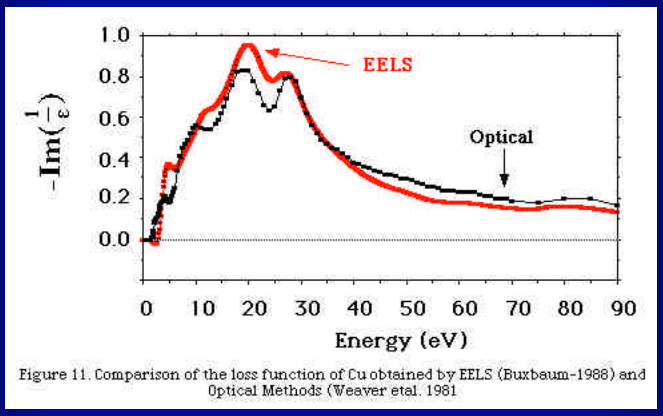

Figure 11. Comparison of the loss function of Cu obtained by EELS (Buxbaum-1988) and Optical Methods (Weaver etal. 1981

Additional EELS Information

Excitation of core levels by the transmitted electron beam can be used to measure the elemental composition of the solid, Near Edge Structure (NES) and EXtended Energy Loss Fine Structure (EXELFS) can be used to elucidate the density of states above the Fermi level and nearest neighbor configurations.

Oxygen K Shell in NiO

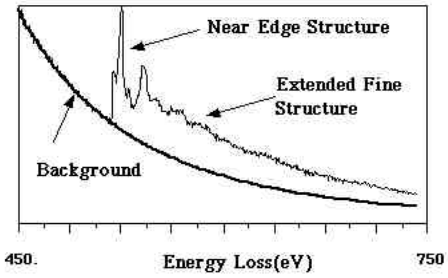

NES as a fingerprint of Chemical State

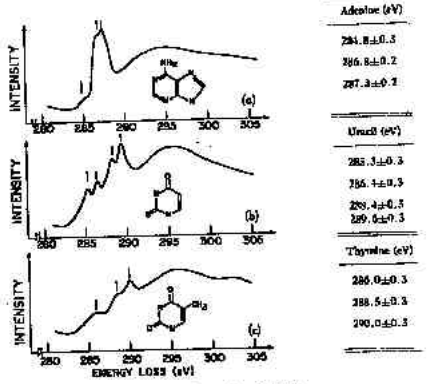

Adenine (eV)
284.8±0.3
286.8±0.2
287.3±0.2

Uracil (eV)
285.3±0.3
286.4±0.3
288.4±0.3
289.6±0.3

Thymine (eV)
285.0±0.3
288.5±0.3
290.0±0.3

Fig. 2. Characteristic electron energy loss spectra of adenine, $C_5N_5H_5$ (a), uracil, $C_4N_2O_2H_4$ (b), and thymine, $C_5N_2O_2H_6$ (c) showing the fine structure in the region of the carbon K-shell ionization edge. The peripheral hydrogen atoms in the chemical structural formulas have been omitted for clarity.

M. Isaacson, J. Chem. Phys. 56,(1972),1803

Copper L-shell Core Loss Spectroscopy in Metallic, Oxide and High Tc Superconductor Phases

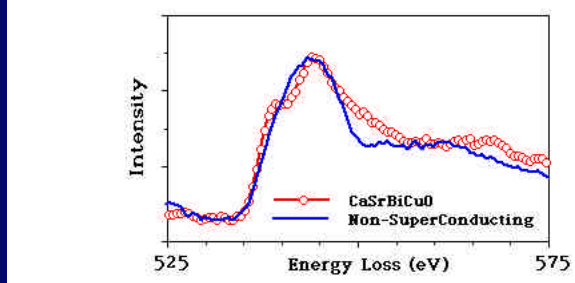

Figure 20. Oxygen K Shell in superconducting and non-superconducting specimens in the $Bi_2Sr_2Ca_{n-1}Cu_nO_x$ system. Note the disappearance of the pre-edge peak in the non-superconducting specimen.

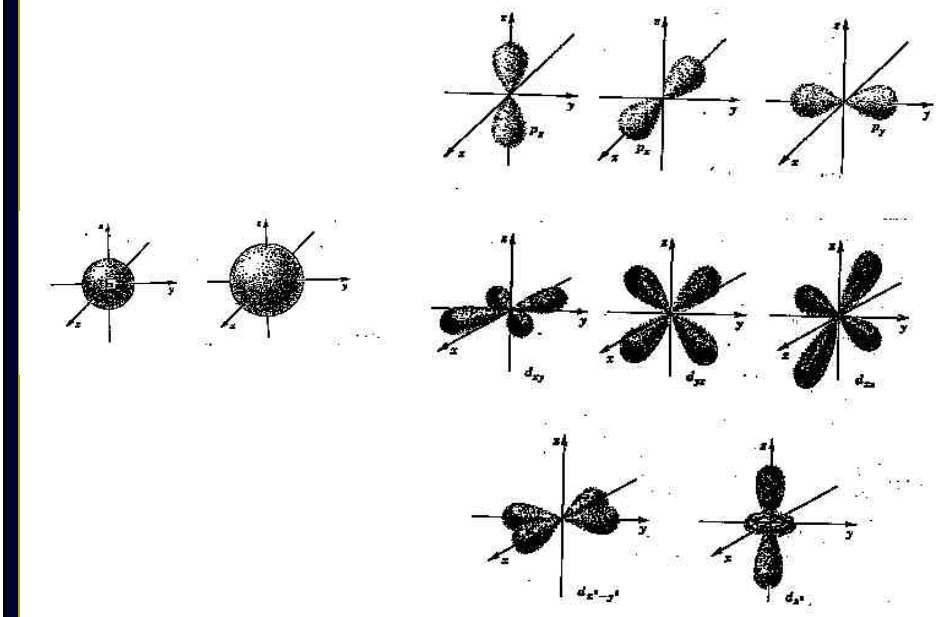

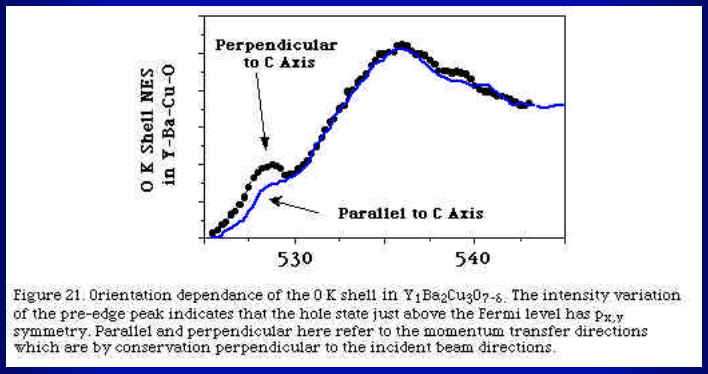

Figure 21. Orientation dependance of the O K shell in $Y_1Ba_2Cu_3O_{7-\delta}$. The intensity variation of the pre-edge peak indicates that the hole state just above the Fermi level has $p_{x,y}$ symmetry. Parallel and perpendicular here refer to the momentum transfer directions which are by conservation perpendicular to the incident beam directions.

Amorphous Fe_xGe_{1-x} Magnetic Materials

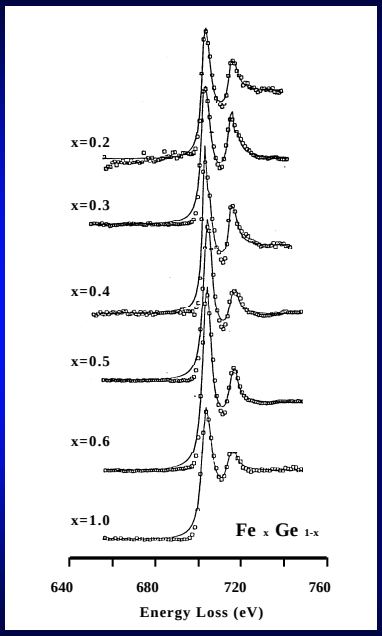

Table 3
Variation in *d-band* occupancy with composition in Fe_xGe_{1-x}

Composition	$h_{Total}/h_{Total}(Fe)$	Ratio $h_{5/2}/h_{3/2}$
1.0	1.0	0.68
0.6	1.3	0.69
0.5	1.1	0.72
0.4	1.1	0.4
0.3	1.3	0.29
0.2	1.0	0.45

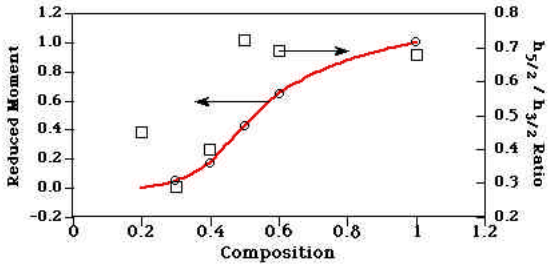

Figure 18 comparison of variation in reduced magnetic moment (open circles) to ratio of $d_{5/2}$ and $d_{5/2}$ holes (squares) as a function of composition in Fe_xGe_{1-x}.

Silicon 111 ZAP- Gamma Corrected

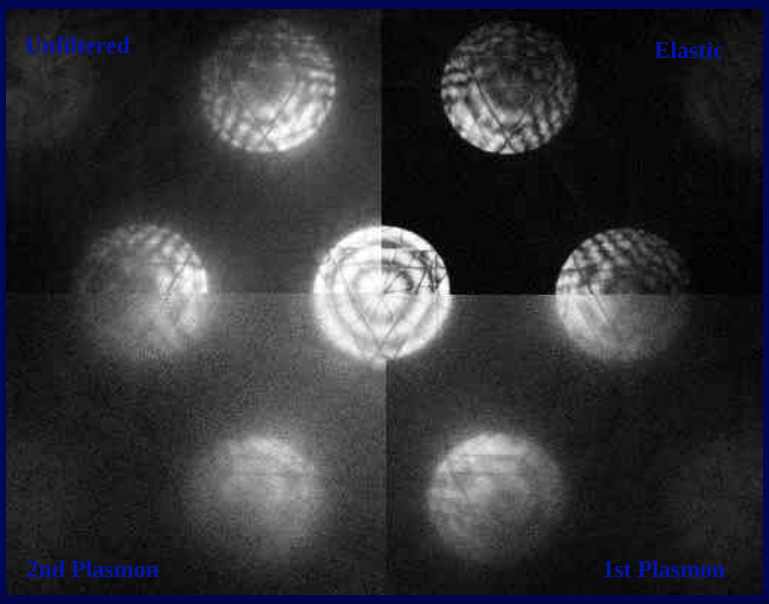

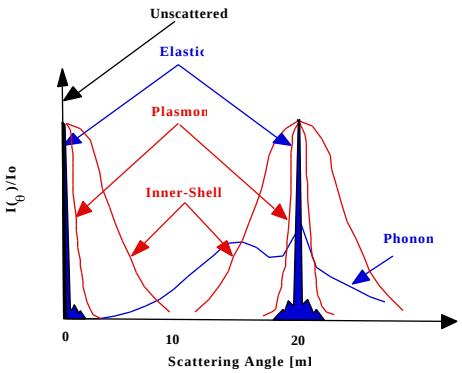

Elastic Scattering : Crystalline Solids

$$\mathbf{I}(\theta) \sim |\mathbf{F(hkl)}|^2$$

$$\mathbf{F(hkl)} = \sum_{\mathbf{j}} \mathbf{f_j(\theta)}\ \mathbf{exp}\ (-2\pi i \vec{g}\cdot\vec{r})$$

$$V(r) = -\sum_{g}^{?} V_g \exp(2\pi i \mathbf{g}.\mathbf{r}) \ ; \ V_g = \frac{h^2}{2\pi m V_e} f(\theta)$$

Energy Filtered Convergent Beam Electron Diffraction

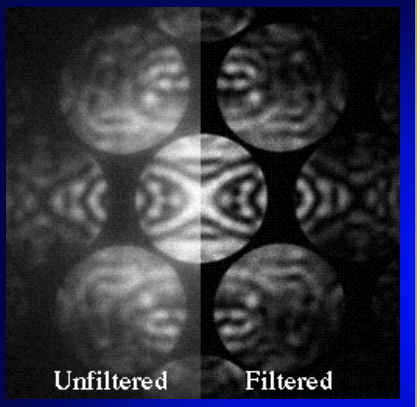

- Filtering Removes Inelastic Scattering
- Dynamical Calculations Used to Compare Experimental Data to Models
- Low Order Structure Factors Determined (Semi-Conductors, Metals)
- Applied to Ti-Al Intermetallics and Charge Density (Difference) Maps

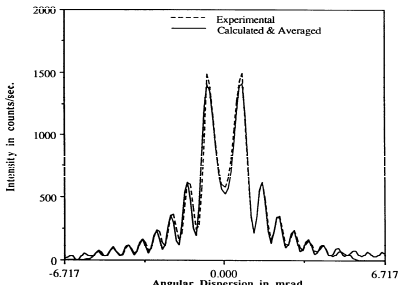

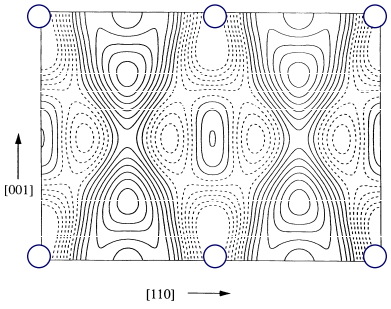

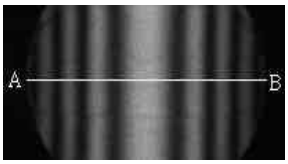

Fig. 1a - (200) CBED dark field disk.

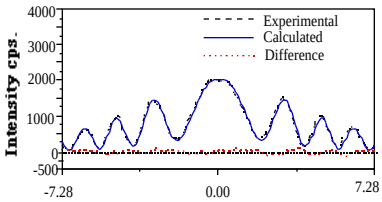

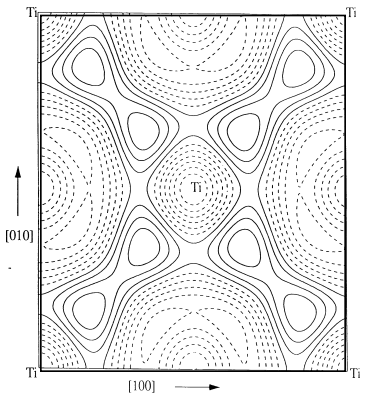

Charge Density Determination
Using Energy Filtered
Convergent Beam Electron Diffraction

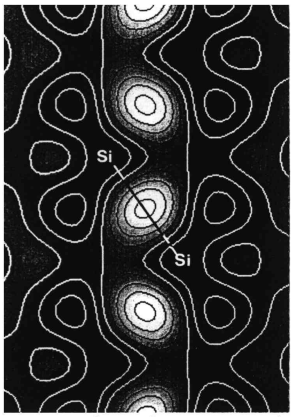

Energy Filtered CBED Results

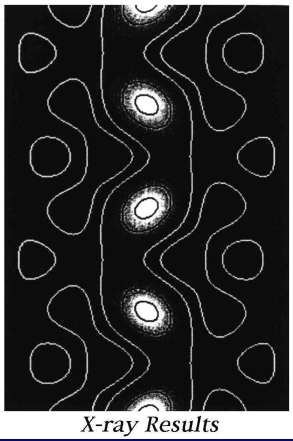

X-ray Results

Radiation Damage in Materials

Damage Creation Event/Process

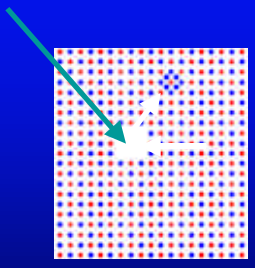

Mobile Vacancy & Interstitials Created

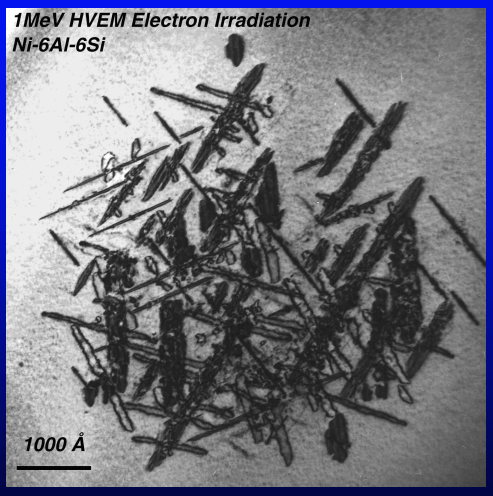

Solid State Order/DisOrder/Amorphization/ Studies

Lindemann Melting Criterion

- *Perfect Crystals Melt:*

$$\langle \mu^2_{vib} \rangle = \frac{9\,\bar{h}^2\,T}{M\,k_B\,\theta_c^2} > \langle \mu^2_{crit} \rangle$$

$$T_m = \frac{M\,k_B\,\theta_c^2}{9\,\bar{h}^2}\,\langle \mu^2_{crit} \rangle$$

- *Defective Crystal Melt :*

$$\langle \mu^2_{total} \rangle = \langle \mu^2_{vib} \rangle + \langle \mu^2_{static} \rangle > \langle \mu^2_{crit} \rangle$$

$$T_d = \frac{M\,k_B\,\theta_d^2}{9\,\bar{h}^2}\,\langle \mu^2_{crit} \rangle$$

Materials Research Society Bulletin : 19 #7 (1994) - Lam & Okamoto

P.C. Liu, P. R. Okamoto,

Solid State Order/DisOrder/Amorphization/ Studies

We can experimentally measure $\langle \mu^2 \rangle$ *using Energy Filtered Electron Diffraction*

$$I(\theta) \sim |F(hkl)|^2 \cdot \{1 - e^{-2M}\}$$

$$M = \frac{8\pi \langle u^2 \rangle \sin(\theta)}{\lambda}$$

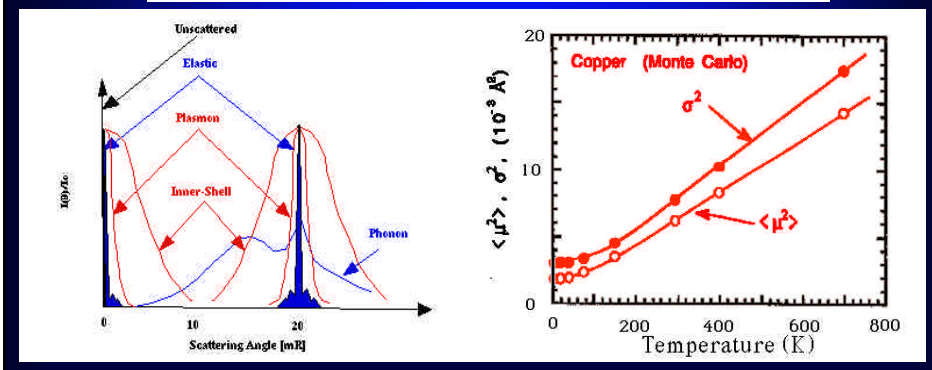

P.C. Liu, P. R. Okamoto,

Energy Filtered Electron Diffraction

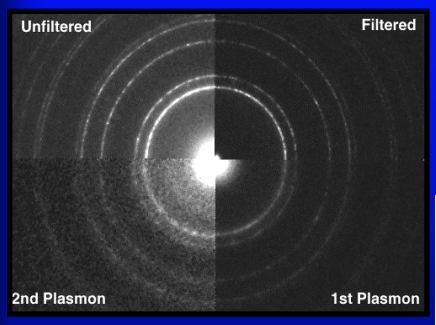

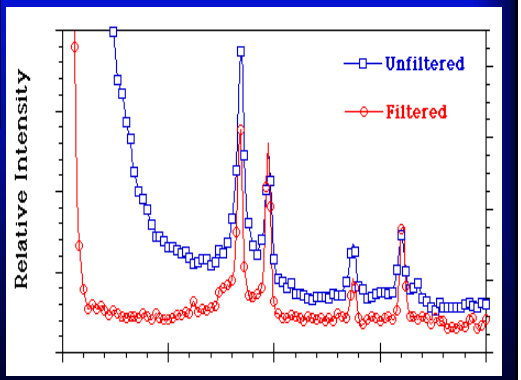

Solid State Order/DisOrder/Amorphization/ Studies

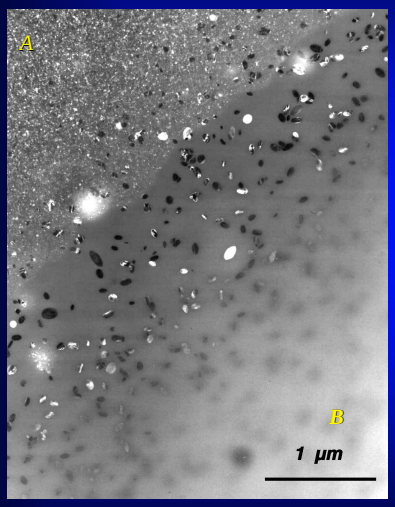

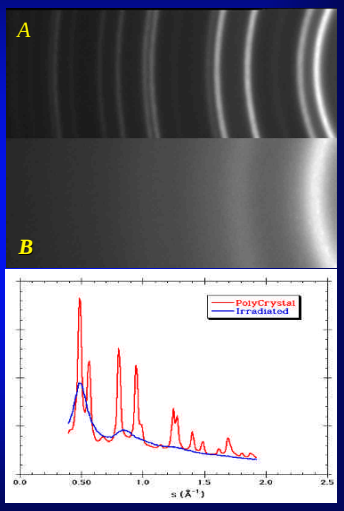

P.C. Liu, P. R. Okamoto,

Solid State Order/DisOrder/Amorphization/ Studies

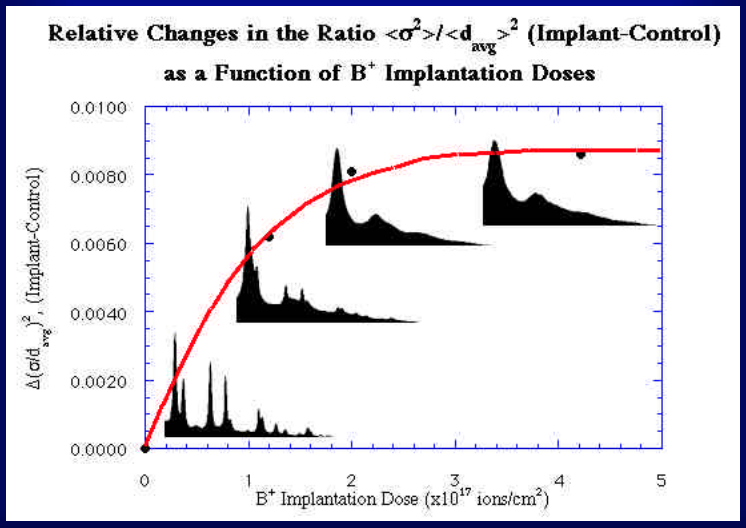

P.C. Liu, P. R. Okamoto,

EELS / NES Measurements
in Order/DisOrder/Amorphization Studies in TM Alloys

Irradition Effects in TM alloys <---> Structure/Properties

Mechanical Properties <---> Electronic Structure

- *TM's have tightly bound valence d band which overlaps and hybridizes with broader nearly Free-electron sp band*
- *In TM's with partially filled d-bands the NES is readily measured.*

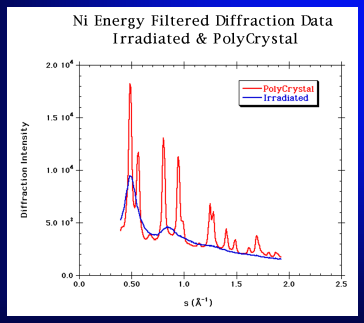

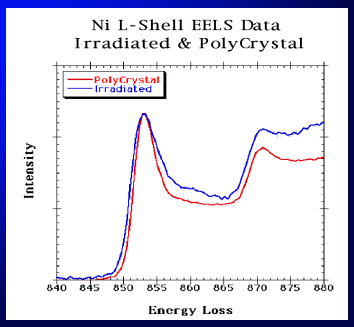

P.C. Liu, P. R. Okamoto,

Phase Stablitiy of Ion Irradiated of Minerals for HLW Storage Materials

Zirconolite ~ Ca $ZrTi_2O_7$

Perovskite ~ Ca Ti O_3

Pyrochlore ~ VIII A_2VI B_2 IV X_6 Y

- Candidate Phases for Immobilization of REE, & ACT in HLW forms
- Over Geologic Time Scales alpha decay causes the minerals to become metamict.
- In-situ Kr Ion Irradiation used in HVEM-Tandem to simulate long-term α-decay damage
  - What is the Polytype, Dose, and Composition dependance?
  - Are there other methods of measuring the damage and can they tell us about the structure?

K.L. Smith

Zirconolite - 2M
Illustrating the loss of crystallinity with irradiation dose (figure 1)

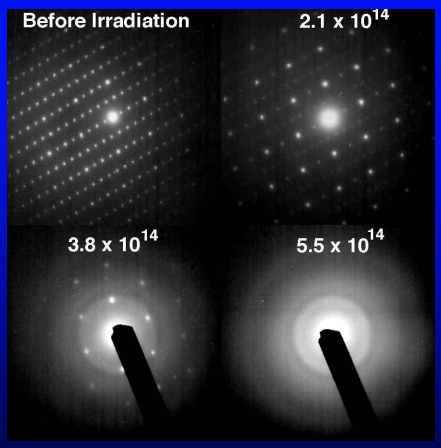

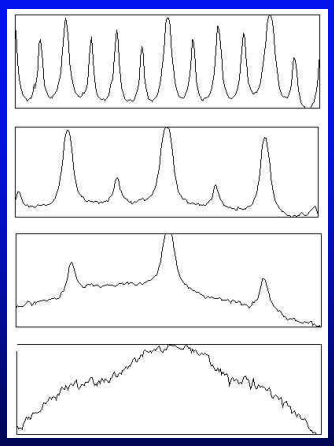

•Selected area diffraction patterns (SADs) of individual grains of various zirconolites were recorded as a function of dose to establish the critical dose for amorphisation (D_c).

Phase Stablitiy of Ion Irradiated of Minerals for HLW Storage Materials

Material	*Dc (10^{14} ions/cm^2)*
Zirconolite - 2M	*5.5*
Nd + Zirconolite- 2M	*5.3*
Nd + Zirconolite - 3T	*3.9*
Nd + Zirconolite - 4M	*3.7*
U + Zirconolite - 2M	*3.8*
U - Pyrochlore	*4.1*
Th - Zirconolite 3T	*6.1*
Perovskite	*17.9*

- *Dc = f (complexity/polytype) = f (dopant) but only by a factor of ~ 2*
- *Additional studies planned*
  - *Vary Ion Energy*
  - *Fabrication Methodology(Sintering/Hot Pressing/Temperature)*
  - *Dopant Partitioning*

K.L. Smith,

EELS Measurements

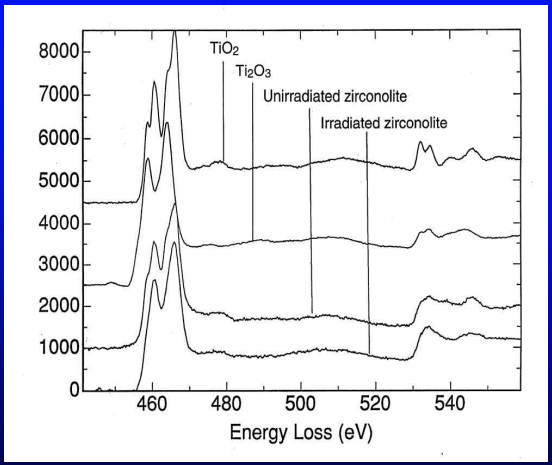

Figure 2. The Ti L edges of undoped zirconolite before and after ion irradiation, and two Ti standards (TiO_2 and Ti_2O_3)

EELS Results

- **Comparison of the Zirconolite and Ti-oxide spectra suggests that Ti predominantly exhibits a valence of 4^+ in both unirradiated and irradiated Zirconolite and that the bond lengths in zirconolite are similar to those in TiO_2. (figure 2)**

- **The electron energy loss near edge structure (ELNES) of the Ti L shell is consistent with the Ti changing from octahedral coordination to tetrahedral coordination (figure 3).**

HR EELS of Zirconolite Ti L shell

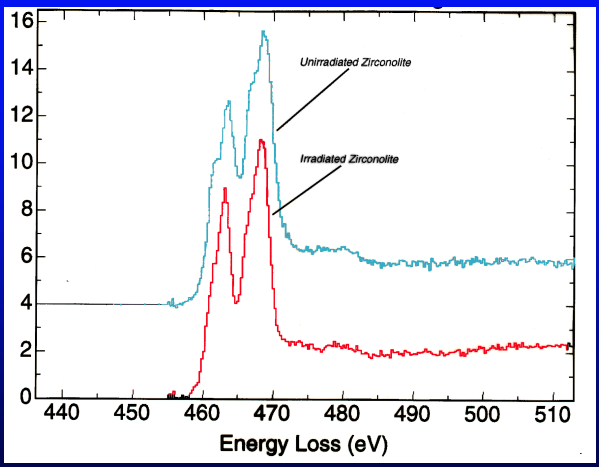

Figure 3. HR EELS of Ti L Shell in Zirconolite.

EELS Results

Specimen	*L_2 /L_3- Spin Orbit*	*L^*_2 /L^*_3- Molecular*	*Energy Shift L_3-L^*_3*
Ti_2O_3	1.25	1.80	2.3
TiO_2	1.45	1.67	2.0
$CaTiO_3$	1.50	1.30	2.5
$(Ca_xGd_y)TiO_3$	1.44	1.50	2.3
$(Ca_xGd_y)(Ti_nAl_m)O_3$	1.42	1.55	2.5
$CaZrTi_2O_7$(Zirconolite)			
UnIrrad.	1.35	1.5	1.9
Irradiated	1.35	1.83	1.4

Table 2

EELS Results

- **To quantitatively measure the changes due to irradiation, we fitted the zirconolite Ti-L spectra with four Lorentzians and calculated L_2/L_3 and L^*_2/ L^*_3 and $L_3 - L^*_{3\ *}$ (Table 2).**
- **L_2/L_3 is the same before and after irradiation which suggests that radiation damage does not significantly affect the number of holes in the d-band (and hence valence).**
- **L^*_2/ L^*_3 increases and $L_3 - L^*_3$ that radiation damage in zirconolite causes a distortion of the octahedral field around Ti atoms toward a tetrahedral configuration**